ADAPTIVE AUTOMOTIVE RADAR DATA ACQUISITION

Anonymous authors
Paper under double-blind review

ABSTRACT

In an autonomous driving scenario, it is vital to acquire and efficiently process data from various sensors to obtain a complete and robust perspective of the surroundings. Many studies have shown the importance of having radar data in addition to images since radar is robust to weather conditions. We develop a novel algorithm for selecting radar return regions to be sampled at a higher rate based on prior reconstructed radar frames and image data. Our approach uses adaptive block-based Compressed Sensing(CS) to allocate higher sampling rates to "important" blocks dynamically while maintaining the overall sampling budget per frame. This improves over block-based CS, which parallelizes computation by dividing the radar frame into blocks. Additionally, we use the Faster R-CNN object detection network to determine these important blocks from previous radar and image information. This mitigates the potential information loss of an object missed by the image or the object detection network. We also develop an end-to-end transformer-based 2D object detection network using the NuScenes radar and image data. Finally, we compare the performance of our algorithm against that of standard CS on the Oxford Radar RobotCar dataset.

1 INTRODUCTION

The intervention of deep learning and computer vision techniques for autonomous driving scenario is aiding in the development of a robust and safe autonomous driving systems. Similar to humans navigating their world with numerous sensors and information, the autonomous driving systems need to process different sensor information efficiently to obtain the complete perspective of the environment to safely maneuver. Numerous studies Meyer & Kuschk (2019), Chang et al. (2020) have shown the importance of having radar data in addition to images for improved object detection performance. The real-time radar data acquisition using compressed sensing is a well-studied field where, even with sub-Nyquist sampling rates, the original data can be reconstructed accurately. During the onboard signal acquisition and processing, compressed sensing will reduce the required measurements, therefore, gaining speed and power savings. In adaptive block-based compressed sensing, based on prior information, important radar blocks would be allocated more sampling resources while maintaining the overall sampling budget the same. This method would further enhance the quality of reconstructed data by focusing on the important regions. In our work, we split the radar into 8 azimuth blocks and used the 2D object detection results from images as prior data to choose the important regions. The 2D object detection network generates the bounding boxes and object classes for objects in the image. The bounding boxes were used to identify the azimuth of the object in radar coordinates. This helped in determining the important azimuth blocks. As a second step, we used both previous radar information and the 2-D object detection network to determine the important regions and dynamically allocate the sampling budget.

Finally, we have also developed an end-to-end transformer-based 2-D object detection Carion et al. (2020) network using the NuScenes Caesar et al. (2020) radar and image dataset. The object detection performance of the model using both Image and Radar data performed better than the object detection model trained only on the image data.

Our main contributions are listed below:

- We have developed an algorithm for selecting important radar return regions to be sampled at a higher rate based on the prior image data processed by the Faster R-CNN object detection network Ren et al. (2015).

- In the extended algorithm, important radar return regions are selected using both object detection output and the previous radar frame.

- We've designed an end-to-end transformer-based 2-D object detection network (DETR-Radar) Carion et al. (2020) using both Nuscenes Caesar et al. (2020) radar and image data.

2 RELATED WORK

The compressed sensing technique is a well-studied method for sub-Nyquist signal acquisition. In Roos et al. (2018), they showed the successful application of standard compressed sensing on radar data with 40% sampling rate. They also showed that they could use a single A/D converter for multiple antennas. In our method, we have shown efficient reconstruction with 10% sampling rate. In another work, Slavik et al. (2016), they used standard compressed sensing based signal acquisition for noise radar with 30% sampling rate. Whereas, we've developed this algorithm for FMCW scanning radar. Correas-Serrano & González-Huici (2018) analysed various compressed sensing reconstruction algorithms such as Orthogonal Matching Pursuit (OMP), Basis Pursuit De-noising (BPDN) and showed that, in automotive settings, OMP performs better reconstruction than the other algorithms. In our algorithm, we have used Basis Pursuit(BP) algorithm for signal reconstruction because, although it is computationally expensive than OMP, BP requires fewer measurements for reconstruction Sahoo & Makur (2015).

The Adaptive compressed sensing technique was used for radar acquisition by Assem et al. (2016). They used the previously received pulse interval as prior information for the present interval to determine the important regions of the pulsed radar. In our first algorithm, we have used only the image data and in the second algorithm, we have used both image and previous radar data on the FMCW scanning radar. In another work, Kyriakides (2011) they used adaptive compressed sensing for a static tracker case and have shown improved target tracking performance. However, in our algorithm, we've used adaptive compressed sensing for radar acquisition from an autonomous vehicle where, both the vehicle and the objects were moving. In Zhang et al. (2012) they used adaptive compressed sensing by optimizing the measurement matrix as a separate least squares problem, in which only the targets are moving. This increases the computational complexity of the overall algorithm. Whereas in our method, the measurement matrix size is increased to accommodate more sampling budget which has the same complexity as the original CS measurement matrix generation technique. In a separate but related work, Nguyen et al. (2019) LiDAR data was acquired based on Region-of-Interest derived from image segmentation results of images. In our work, we have acquired radar data using 2-D object detection results.

Apart from radar, adaptive CS was used for images and videos. In Mehmood et al. (2017), the spatial entropy of the image helped in determining the important regions. The important regions were then allocated more sampling budget than the rest which improved reconstruction quality. In another work, Zhu et al. (2014), the important blocks were determined based on the variance of each block, the entropy of each block and the number of significant Discrete Cosine Transform (DCT) coefficients in the transform domain. In Wells & Chatterjee (2018), object tracking across frames of a video was preformed using Adaptive CS. The background and foreground segmentation helped in allocating higher sampling density to the foreground and very low sampling density to the background region. Liu et al. (2011) similarly used adaptive CS for video acquisition based on inter-frame correlation. Also, Ding et al. (2015), performed the joint CS of two adjacent frames in a video based on the correlation between the frames.

Finally, there were numerous studies that showed the advantage of using both radar and images in an object detection network for improved object detection performance. Nabati & Qi (2019) used radar points to generate region proposals for Fast R-CNN object detection network which made the model faster than the selective search based region proposal algorithm in Fast R-CNN. Nobis et al. (2019), Chadwick et al. (2019) showed that radar in addition to image improved distant vehicle object detection and occluded object detection due to adverse weather conditions. In Chang et al. (2020), spatial attention was used to combine radar and image features for improved object detection using FCOS Tian et al. (2019) object detection network.

3 METHOD

3.1 DATASET

The Oxford Radar RobotCar dataset Barnes et al. (2019) consists of various sensor readings while the vehicle was driven around Oxford, UK in January 2019. The vehicle was driven for a total of 280km in an urban driving scenario. We have used camera information from the centre captured with Point Grey Bumblebee XB3 at 16 Hz, rear data captured by Point Grey Grasshopper2 at 17 Hz. The Radar data was collected by NavTech CT350-X, Frequency Modulated Continuous-Wave scanning radar with 4.38 cm range resolution and 0.9 degrees in rotation resolution at 4 Hz. They captured radar data with a total range of 163m. In addition to this, they have released the ground-truth radar odometry. However, in our case, we require 2D object annotation on the radar data to validate our approach. Since this a labor-intensive task, we have chosen 3 random scenes from the Oxford dataset, each with 10 to 11 radar frames and have marked the presence or absence of the target object across reconstructions. To the best of our knowledge, this is the only publicly available raw radar dataset. Hence, we used this dataset for testing our compressed sensing algorithm.

In order to train our DETR-Radar object detection model, we used the NuScenes v0.1 dataset Caesar et al. (2020). This is one of the publicly available datasets for autonomous driving with a range of sensors such as Camera, LiDAR and radar with 3D bounding boxes. Similar to Nabati & Qi (2019), we have converted all the 3D bounding box annotations to 2D bounding boxes and merged similar classes to 6 total classes, Car, Truck, Motorcycle, Person, Bus and Bicycle. This dataset consists of around 45k images and we have split the dataset into 85% training and 15% validation.

3.2 ADAPTIVE BLOCK-BASED COMPRESSED SENSING

Compressed Sensing is a technique where, if the original signal x, with $x \in R^N$, the measurement y is taken using the measurement matrix ϕ, using $y = \phi x$, where, $\phi \in R^{(MXN)}$ and $y \in R^M$ with an effective number of measurements, $M << N$. The theory, Mehmood et al. (2017) guarantees that if the input is K-sparse in some domain, the data, with a high probability can be recovered from $O(KlogN)$ measurements. In order to recover the signal from y, we used Basis Pursuit(BP) algorithm. We used binary sparse matrix as the measurement matrix He et al. (2010) since it promotes easy hardware implementation. In our case, we assumed that the data is sparse in DCT domain. The BP algorithm uses l_1 norm to recover the data using, $min_x||\theta x||_1 \ s.t. \ \phi x = y$, where, θ is the domain transformation matrix. The radar data is split into 50x100 blocks and CS is applied to each block. However, depending on the importance of a block, the number of measurements M is increased dynamically while maintaining the total budget as 10% sampling rate.

3.3 ALGORITHM 1

The front camera generates images at 16 Hz, the rear camera at 17 Hz and radar frames are acquired at 4 Hz. The object detection network takes 0.12s per image to generate bounding boxes and object class for a particular image. This algorithm is designed to access object information from images 0.18s before the radar frame acquisition timestamp to account for processing the image to get the bounding boxes and object classes. The front camera has 66 degrees horizontal Field-of-View (HFoV). The rear camera has 180 degrees HFoV. The radar data covers the entire 360 degrees HFoV. Therefore, at a given timestamp, from the camera image, we have information about the rear surrounding of 180 degrees plus the front of 66 degrees. From this technique, there would be a blind spot of 57 degrees to the left and 57 degrees to the right. However, this would be mitigated in Algorithm 2.

In our method, we are performing an adaptive block-based CS. The radar data is split into 8 equal regions, in azimuth and 37 equal regions in range. This creates a block of size 50x100. Therefore, from the camera image, the important azimuth sections to focus on would be derived based on the presence of an objects in that section. Since the depth information is not available from the camera images, in this case, we can only choose azimuth sections and not the range. The chosen sections were dynamically allocated more sampling rate than the others. Also, since the radar data was acquired with 163 m range, we have allocated more sampling rate the first 18 range blocks compared to the last 19 since there is not much useful information in the farther range values. The

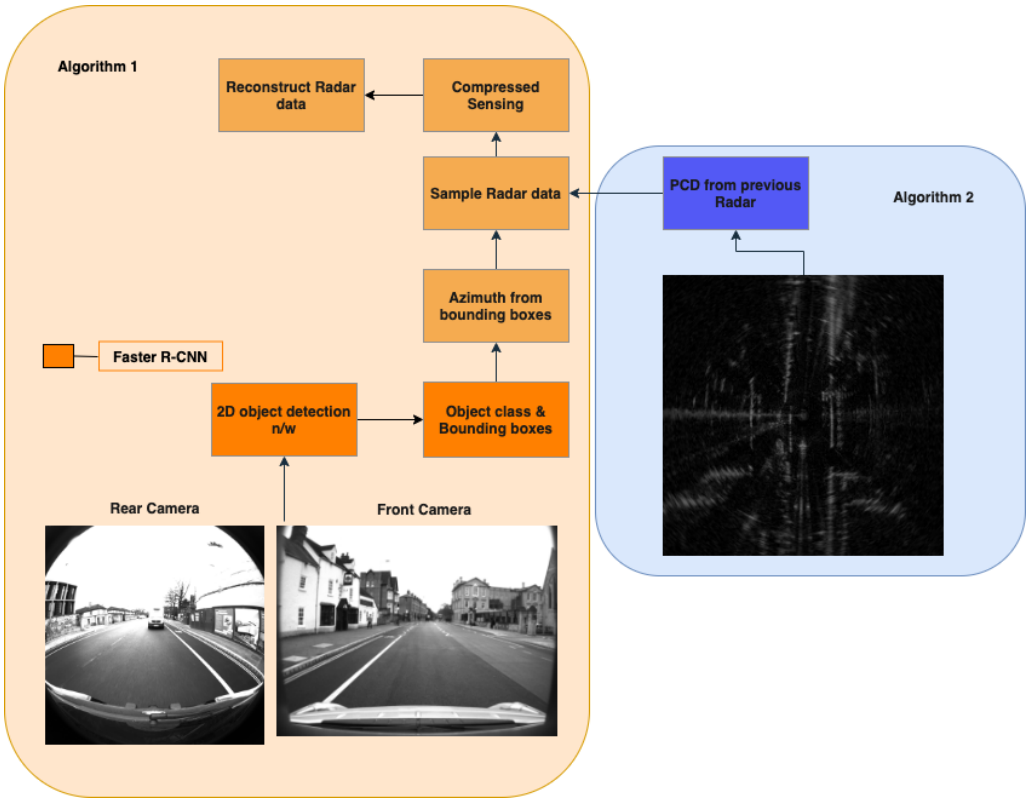

Figure 1: The overview of Algorithm 1 and Algorithm 2. Algorithm 1 takes front and rear camera data as input to identify the important azimuth blocks. Algorithm 2 samples radar data based on azimuth from images and the previous radar frame.

average driving speed in an urban environment is 40 miles per hour. Since radar is captured at 4 Hz, for every frame, the object could have moved 4.25m. Since the bin resolution is 4.38cm and for a particular block with 100 bins, the area spanned would be 4.38m. Since we are looking into the first 18 range blocks, that covers a total area of 78.84m. Hence, in an urban setting, the moving vehicle can be comfortably captured by focusing within the 78.84m range. In a freeway case, for an average speed of 65 miles per hour, the vehicle could have moved 7.2m per frame and again, this would be captured by focusing on the first 78.84m. Algorithm 1 steps:

1. Acquire front and rear camera information at t=0s.
2. Process them simultaneously through the Faster R-CNN network and generate results at t=0.12s.
3. Process the Faster R-CNN results to determine the important azimuth blocks for radar.
4. Dynamically allocate more sampling rate to the chosen azimuth blocks and fewer to the other blocks while maintaining the total sampling budget.
5. Acquire the radar data at t=0.25s based on the recommenced sampling rate.

3.4 ALGORITHM 2

However, in order to avoid the effects of the blind spot region of the camera, the lost information from the camera due to weather or other effects and object missed by the object detection network, we have designed the extended algorithm to utilize the previous radar information to sample the current radar frame. In order to maintain the bit budget, the chosen range blocks for a particular azimuth is further limited to 14, covering 61.32m in range. Therefore, the balance sampling budget is used to provide a higher sampling rate to the chosen blocks from algorithm 2. Algorithm 2 steps:

1. Repeat steps 1 to 5 from algorithm 1 for frame 1.
2. Repeat steps 1 to 3 from algorithm 1.
3. Using the Constant False Alarm Rate (CFAR) Richards (2005) detection algorithm, the blocks with point clouds from radar data are additionally chosen to have a higher sampling rate.
4. Acquire the radar data based on the above allocation.

As shown in figure 1, Algorithm 1 takes rear and front camera images and predicts object class and bounding boxes. The object's x coordinate in the front camera image is converted from the cartesian plane to azimuth ranging from -33 to 33 degrees corresponding to the HFoV of the front camera. The object's x coordinate from the rear camera is converted to azimuth ranging from 90 to 270 degrees. Therefore, if an object is present in one of the 8 azimuth blocks, divided as 0-45 degrees, 45-90 degrees and so on, that azimuth block is considered important and allocated more sampling rate. Algorithm 2 is an extension of Algorithm 1, in addition to azimuth, if a radar point cloud is detected in any of the blocks (50x100), they are marked necessary and were allocated more sampling rate. In the experiments section, we have shown cases where the radar point clouds helped in identifying objects present in the camera's blind spot.

3.5 DETR-RADAR

The Faster R-CNN Ren et al. (2015) object detection network is one of the well-refined techniques for 2D object detection. However, it relies heavily on two components, non-maximum suppression and anchor generation. The end-to-end transformer-based 2D object detection introduced in Carion et al. (2020), eliminates the need for these components. We included radar data in two ways. In the first case, we included the radar data as an additional channel to the image data Nobis et al. (2019). In the second case, we rendered the radar data on the image. We used perspective transformation based on Nabati & Qi (2019) to transform radar data points from the vehicle coordinates system to camera-view coordinates. The models where radar data were included as an additional channel were trained for longer duration since the first layer of the backbone structure had to be changed to accommodate the additional channel. In all the above cases, the models were pre-trained on the COCO dataset and we fine-tuned them on the NuScenes data. To the best of our knowledge, we are the first ones to implement end-to-end transformer based 2D object detection using both image and radar data.

4 EXPERIMENTS

In order the validate our approach, we tested it on 3 scenes from the Oxford radar robot car dataset. The image data was processed using the Faster R-CNN object detection network Girshick et al. (2018) to obtain object classes and 2D bounding boxes. ResNet-101 was used as the backbone structure, which was pre-trained on the ImageNet dataset Russakovsky et al. (2015). The faster R-CNN network was trained on the COCO train dataset and gave 39.8 box AP on the COCO validation dataset. Since the model was originally trained on the COCO dataset, it predicts 80 classes. However, we filtered pedestrians, bicycle, car and truck classes from the predictions for a given scene. In order to capture and present the radar data clearly, we have shown data for a range of 62.625m from the autonomous vehicle. Although the original radar data is captured for a range of 163m, we could find meaningful information in the first 62.625m. The total sampling budget was set to 10%. Therefore, baseline reconstruction was uniformly provided with 10% sampling rate for all the blocks.

In algorithm 1, we split the radar into three regions. R1: The chosen azimuth until 18th range block (78.84m), R2: the other azimuth regions until the 18th range block (78.84m) and finally, R3: all the azimuth blocks from 19th to 37th range block. In general, from the images, the chosen azimuth ranges from 3 to 6 out of 8. If there were only 3 azimuth blocks chosen, we randomly sampled one more azimuth block. Therefore, when there were 4 azimuth blocks, R1 was sampled at 30.8%, R2 at 5% and R3 at 2.5% sampling rate. In the case of 5 azimuth blocks, R1 was sampled at 25.5%, R2 and R3 at 5% and 2.5% respectively. In the case of 6 azimuths, R1 at 20.2%, R2 at 5% and R3 at 2.5%.

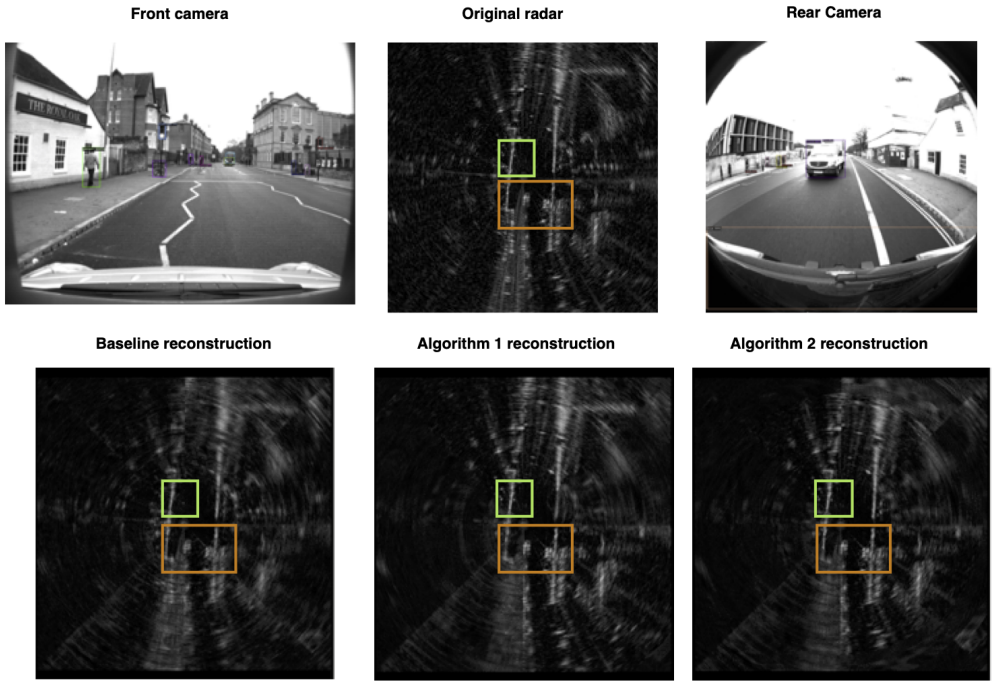

Figure 2: The figure above is from Scene 1, frame 10. In the top row, we show the front image data and rear image processed by the 2D object detection network. The original radar corresponds to the raw radar data acquired in the scene. The green box on the radar data, when zoomed in, would show the person to the left on the front camera. The person is not visible on the baseline reconstruction but can be seen in our reconstruction. The orange box highlights the pedestrians and the truck on the rear image. In general, due to a higher sampling budget, in our reconstruction, the truck and pedestrians are sharper.

In algorithm 2, the regions were again split into 3. However, R1: The chosen azimuth until 14th range (61.32m) while R2 and R3 were the same from the previous algorithm. The previous reconstructed radar frame was processed by the CFAR detector to identify point clouds corresponding to objects. If a radar block had a point cloud, they were classified as important. The sampling budget saved from R1 was used to sample radar blocks classified as important from the previous radar frame. In table 1, we have discussed the presence or absence/faint visibility of an object in a frame across reconstructions. Apart from that, in all frames across scenes except for frame 2, scene 3 truck reconstruction, the mentioned objects were sharper in our reconstruction compared to the baseline. The radar images have been enhanced for better visibility of objects.

In the first scene, the autonomous vehicle moved across an almost straight street without turning. There was a vehicle behind it and pedestrians on the right sidewalk and a pedestrian on the left sidewalk to the front. As shown in table 1, the person on the top left is not visible or very faint on the baseline reconstruction on frame 2 to 10. However, the person is visible on both the Algorithm 1 and Algorithm 2 reconstructions. In frame 2, the pedestrians on the right side happened to be in the blind spot of both the front and rear cameras. Therefore, the reconstruction of Algorithm 1 on that segment was poor. However, that region was captured from the previous radar frame and a higher sampling rate was allocated to region with pedestrians and it was reconstructed appropriately using Algorithm 2. Apart from the listed objects in the table, the rear vehicle was, in general, sharper than baseline reconstruction in all the frames reconstructed using Algorithm 1 and Algorithm 2.

In scene 2, the vehicle waited on the side of an intersection for a truck to pass by. This truck is visible in all the reconstructions. In frame 2, the car was in the blind spot and it was missed by the CFAR in the previous radar frame as well as the image. Therefore, it is visible in the baseline and it was not reconstructed by our algorithm. In frames 4-6 and 8, the car to the rear right was missed by the camera. But, it was captured in algorithm 2 and was sharper than the baseline reconstruction.

Scene	Frame	Object	Baseline	Algorithm 1	Algorithm 2
Scene 1	1	Person (top-left)	no	yes	-
	2-10	Person (top-left)	no	yes	yes
	2	Pedestrians(rear)	yes	no	yes
Scene 2	7	car (top-left)	no	yes	yes
	6-11	Bicycle (rear)	no	yes	yes
	2	car (rear-right)	yes	no	no
	4-6,8	car (rear-right)	yes	no	yes
	4-7	Pedestrian (rear-left)	no	yes	yes
	9-11	Car(rear-left)	yes	no	yes
Scene 3	2-6	car (rear)	no	yes	yes
	2-4	car (top-right)	no	yes	yes
	8	car (rear-right)	no	yes	yes

Table 1: The table highlights the presence of an object as 'yes' and if the object is very faint or absent, it is indicated as 'no'.

Again, in frames 9-11, the car to the rear left was missed by the object detection network. But, it was captured from the previous radar frame and it was reconstructed by Algorithm 2 with a higher sampling rate. Apart from this the reconstruction of radar data for the car to the front of the vehicle, pedestrian at the rear of the vehicle by Algorithm 1 and Algorithm 2 were sharper than the baseline reconstruction.

In scene 3, the vehicle crossed a traffic signal. There was a bus to the left, another bus to the front and a car passed by on the opposite direction. There were a few cars behind the vehicle. In all the frames, the buses were captured by all the reconstruction schemes. However, our algorithm gave sharper results. As shown in the table 1, the cars behind the autonomous vehicle were captured by our algorithms. However, it was not captured by the baseline reconstruction. The result is highlighted using an orange box in figure 3. Similarly, the car passing by on the opposite side was captured by our algorithm and it is barely visible in the baseline reconstruction and it is highlighted using a green box in figure 3. In raw radar, the poles and buildings tend to have a sharper appearance than cars or pedestrians based on the size or position of the cars and pedestrians. Therefore, the car is the tiny region right below the bus and building, highlighted by the green box. This validates the necessity to allocate a higher sampling budget for important objects such as pedestrians or cars on the road.

Finally, we trained a separate object detection network using the NuScenes image and radar data. All of our models were trained on the COCO detection dataset and we fine-tuned them on the Nuscenes v0.1 dataset. As shown in the table 2, our baseline comparison is with the Nabati & Qi (2019) paper, where, they trained the model on Nuscenes v0.1 image dataset and used the radar data for anchor generation. The Faster R-CNN Img and Faster R-CNN RonImg models had ResNet-101 He et al. (2015) as the backbone structure Girshick et al. (2018). The models with Img+R were trained with radar as an additional channel. Therefore, the first layer of the backbone structure was changed to process the additional radar channel. The DETR network Carion et al. (2020) had ResNet-50 He et al. (2015) as the backbone structure, a transformer encoder, transformer decoder followed by a 3-layer feed-forward bounding box predictor. The Img and RonImg models were trained for the same number of epochs for a fair comparison. The Img+R models were trained for additional epochs since the backbone structure's first layer was modified. In the Faster R-CNN case, Img+R has better performance than Img. While, in DETR, RonImg has better performance. The Faster R-CNN Img and RonImg were trained for 25k iterations. The Faster R-CNN Img+R was trained for 125k iterations. DETR Img and DETR RonImg models were trained for 160 epochs. While DETR Img+R was trained for 166 epochs. The DETR - RonImg model performed better across various metrics compared to the baseline, Faster R-CNN and DETR Img+R model. We believe that the attention heads in the transformer architecture helped in focusing object detection predictions around the radar points. However, the Faster R-CNN Img+R was better than Faster R-CNN RonImg model. We used the standard evaluation metrics, mean average precision (AP), mean average recall (AR), average precision at 0.5, 0.75 IOU, small, medium and large AR Lin et al. (2015).

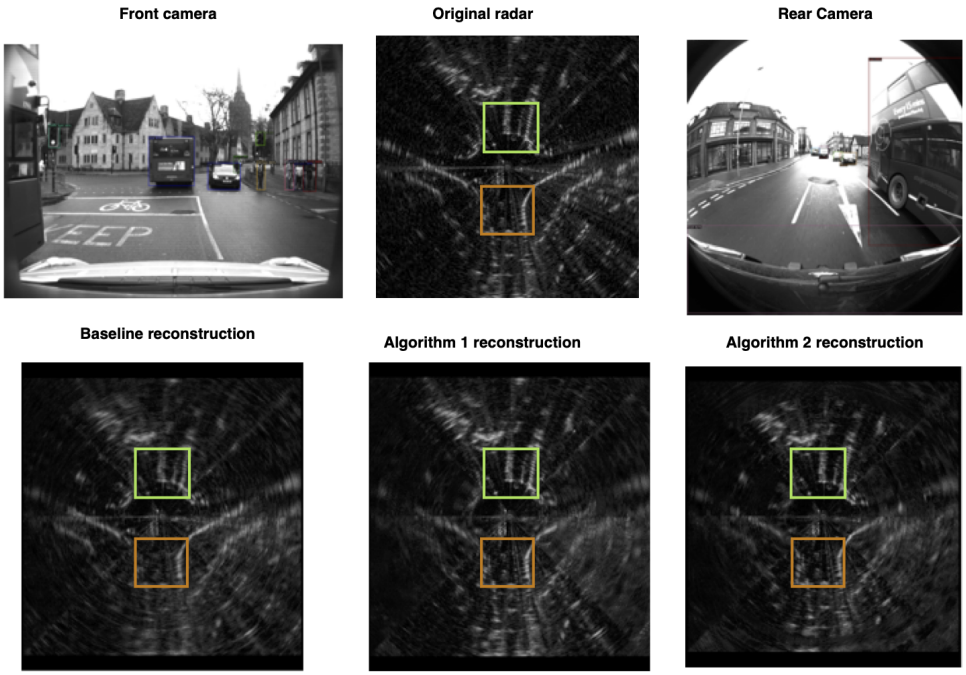

Figure 3: The figure above is from Scene 3, frame 2. The green box when zoomed in shows the car passing by to the right of the autonomous vehicle right below the front bus and radar returns from the wall. The orange box highlights the car behind the autonomous vehicle, captured by our algorithms and missed by the baseline.

Network	AP	AP50	AP75	AR	ARs	ARm	ARl
Fast R-CNN Nabati & Qi (2019)	0.355	0.590	0.370	0.421	0.211	0.391	0.514
Faster R-CNN - Img	0.395	0.678	0.417	0.470	0.256	0.444	0.568
Faster R-CNN - Img+R	0.462	0.738	0.503	0.530	0.328	0.515	0.599
Faster R-CNN - RonImg	0.380	0.654	0.400	0.449	0.176	0.421	0.563
DETR - Img	0.471	0.802	0.504	0.616	0.384	0.572	0.725
DETR - RonImg	0.486	0.804	**0.527**	**0.636**	0.401	**0.602**	0.731
DETR - Img+R	0.448	0.763	0.468	0.582	0.297	0.549	0.688

Table 2: Img denotes model trained on Images, Img + R indicated model trained with Radar as an additional channel and RonImg is for a model trained with the radar rendered on image.

5 Conclusion

We have shown that adaptive block-based CS using the prior image and radar data aided in the sharper reconstruction of radar data. In algorithm 1, we used the prior image data to distribute a higher sampling rate on important blocks. The objects that were either missed by the image or the object detection network was effectively captured by the previous radar frame and were reconstructed with a higher sampling rate. Our end-to-end transformer based model trained on image and radar has better object detection performance than Faster R-CNN and transformer-based model trained on just images, validating the necessity for radar in addition to images. Similar to image data aiding in sampling radar data efficiently, this method *could* be extended to other modalities. Where, if an object's location is predicted by radar, it could help in sampling LiDAR data efficiently.

REFERENCES

A. M. Assem, R. M. Dansereau, and F. M. Ahmed. Adaptive sub-nyquist sampling based on haar wavelet and compressive sensing in pulsed radar. In *2016 4th International Workshop on Compressed Sensing Theory and its Applications to Radar, Sonar and Remote Sensing (CoSeRa)*, pp. 173–177, 2016.

Dan Barnes, Matthew Gadd, Paul Murcutt, Paul Newman, and Ingmar Posner. The oxford radar robotcar dataset: A radar extension to the oxford robotcar dataset, 2019.

Holger Caesar, Varun Bankiti, Alex H. Lang, Sourabh Vora, Venice Erin Liong, Qiang Xu, Anush Krishnan, Yu Pan, Giancarlo Baldan, and Oscar Beijbom. nuscenes: A multimodal dataset for autonomous driving, 2020.

Nicolas Carion, Francisco Massa, Gabriel Synnaeve, Nicolas Usunier, Alexander Kirillov, and Sergey Zagoruyko. End-to-end object detection with transformers, 2020.

S. Chadwick, W. Maddern, and P. Newman. Distant vehicle detection using radar and vision. In *2019 International Conference on Robotics and Automation (ICRA)*, pp. 8311–8317, 2019.

Shuo Chang, Yifan Zhang, Fan Zhang, Xiaotong Zhao, Sai Huang, Zhiyong Feng, and Zhiqing Wei. Spatial attention fusion for obstacle detection using mmwave radar and vision sensor. *Sensors (Basel, Switzerland)*, 20(4), February 2020. ISSN 1424-8220. doi: 10.3390/s20040956. URL https://europepmc.org/articles/PMC7070402.

A. Correas-Serrano and M. A. González-Huici. Experimental evaluation of compressive sensing for doa estimation in automotive radar. In *2018 19th International Radar Symposium (IRS)*, pp. 1–10, 2018.

X. Ding, W. Chen, and I. Wassell. Block-based feature adaptive compressive sensing for video. In *2015 IEEE International Conference on Computer and Information Technology; Ubiquitous Computing and Communications; Dependable, Autonomic and Secure Computing; Pervasive Intelligence and Computing*, pp. 1675–1680, 2015.

Ross Girshick, Ilija Radosavovic, Georgia Gkioxari, Piotr Dollár, and Kaiming He. Detectron. https://github.com/facebookresearch/detectron, 2018.

Kaiming He, Xiangyu Zhang, Shaoqing Ren, and Jian Sun. Deep residual learning for image recognition, 2015.

Z. He, T. Ogawa, and M. Haseyama. The simplest measurement matrix for compressed sensing of natural images. In *2010 IEEE International Conference on Image Processing*, pp. 4301–4304, 2010.

I. Kyriakides. Adaptive compressive sensing and processing for radar tracking. In *2011 IEEE International Conference on Acoustics, Speech and Signal Processing (ICASSP)*, pp. 3888–3891, 2011.

Tsung-Yi Lin, Michael Maire, Serge Belongie, Lubomir Bourdev, Ross Girshick, James Hays, Pietro Perona, Deva Ramanan, C. Lawrence Zitnick, and Piotr Dollár. Microsoft coco: Common objects in context, 2015.

Z. Liu, A. Y. Elezzabi, and H. V. Zhao. Maximum frame rate video acquisition using adaptive compressed sensing. *IEEE Transactions on Circuits and Systems for Video Technology*, 21(11): 1704–1718, 2011.

Irfan Mehmood, Ran Li, Xiaomeng Duan, Xiaoli Guo, Wei He, and Yongfeng Lv. Adaptive compressive sensing of images using spatial entropy. *Computational Intelligence and Neuroscience)*, 2017. doi: 10.1155/2017/9059204. URL https://doi.org/10.1155/2017/9059204.

M. Meyer and G. Kuschk. Deep learning based 3d object detection for automotive radar and camera. In *2019 16th European Radar Conference (EuRAD)*, pp. 133–136, 2019.

R. Nabati and H. Qi. Rrpn: Radar region proposal network for object detection in autonomous vehicles. In *2019 IEEE International Conference on Image Processing (ICIP)*, pp. 3093–3097, 2019.

X. T. Nguyen, K. Nguyen, H. Lee, and H. Kim. Roi-based lidar sampling algorithm in on-road environment for autonomous driving. *IEEE Access*, 7:90243–90253, 2019.

F. Nobis, M. Geisslinger, M. Weber, J. Betz, and M. Lienkamp. A deep learning-based radar and camera sensor fusion architecture for object detection. In *2019 Sensor Data Fusion: Trends, Solutions, Applications (SDF)*, pp. 1–7, 2019.

Shaoqing Ren, Kaiming He, Ross Girshick, and Jian Sun. Faster r-cnn: Towards real-time object detection with region proposal networks, 2015.

Mark Richards. Fundamentals of radar signal processing, 2005.

F. Roos, P. Hügler, C. Knill, N. Appenrodt, J. Dickmann, and C. Waldschmidt. Data rate reduction for chirp-sequence based automotive radars using compressed sensing. In *2018 11th German Microwave Conference (GeMiC)*, pp. 347–350, 2018.

Olga Russakovsky, Jia Deng, Hao Su, Jonathan Krause, Sanjeev Satheesh, Sean Ma, Zhiheng Huang, Andrej Karpathy, Aditya Khosla, Michael Bernstein, Alexander C. Berg, and Li Fei-Fei. Imagenet large scale visual recognition challenge, 2015.

S. K. Sahoo and A. Makur. Signal recovery from random measurements via extended orthogonal matching pursuit. *IEEE Transactions on Signal Processing*, 63(10):2572–2581, 2015.

Z. Slavik, A. Viehl, T. Greiner, O. Bringmann, and W. Rosenstiel. Compressive sensing-based noise radar for automotive applications. In *2016 12th IEEE International Symposium on Electronics and Telecommunications (ISETC)*, pp. 17–20, 2016.

Zhi Tian, Chunhua Shen, Hao Chen, and Tong He. Fcos: Fully convolutional one-stage object detection, 2019.

J. W. Wells and A. Chatterjee. Content-aware low-complexity object detection for tracking using adaptive compressed sensing. *IEEE Journal on Emerging and Selected Topics in Circuits and Systems*, 8(3):578–590, 2018.

J. Zhang, D. Zhu, and G. Zhang. Adaptive compressed sensing radar oriented toward cognitive detection in dynamic sparse target scene. *IEEE Transactions on Signal Processing*, 60(4):1718–1729, 2012.

S. Zhu, B. Zeng, and M. Gabbouj. Adaptive reweighted compressed sensing for image compression. In *2014 IEEE International Symposium on Circuits and Systems (ISCAS)*, pp. 1–4, 2014.